Modeling the Electrophoresis of Peptides and Proteins: Improvements in the "Bead Method" to Include Ion Relaxation and "Finite Size Effects"

Yao Xin, Richard Hess, Nhi Ho, and Stuart Allison*

Department of Chemistry, Georgia State University, Atlanta, Georgia 30302-4098

Received: August 7, 2006; In Final Form: October 2, 2006

A bead model methodology developed in our lab (Xin et al. *J. Phys. Chem. B* **2006**, *110,* 1038) and applicable to modeling the free solution electrophoretic mobility of peptides and proteins is generalized in two significant ways. First, an approximate account is taken of the relaxation effect, which makes the methodology applicable to more highly charged peptides and proteins than was previously possible. Second, a more accurate account is taken of the finite size of the beads making up the model structure. This improvement makes the method applicable at higher salt concentrations and/or to models consisting of larger sized subunits. The relaxation effect is accounted for by correcting "unrelaxed" mobilities on the basis of model size and average electrostatic surface, or ζ potential. Correction factors are estimated using those of spheres with the same hydrodynamic radius and ζ potential as the model structure. The correction factors of spheres are readily determined. The more general methodology is first applied to two sets of peptides (74 different peptides total) varying in size from 2 to 42 amino acids. The sets also cover a wide range of net charges. It is shown that accounting for finite bead size results in a small change in model mobilities under the conditions of the experiments (35 mM monovalent salt). The correction for ion relaxation, however, can be significant for highly charged peptides and improves agreement between model and experimental mobilities. Our correction procedure is also tested by examining the electrophoretic mobility of a particular protein "charge ladder" (Carbeck et al. *J. Am. Chem. Soc*. **1999**, *121*, 10 671), where the protein charge is varied over a wide range yet the conformation remains essentially constant. In summary, the effects of ion relaxation can be significant if the absolute electrophoretic mobility of a peptide exceeds approximately 0.20 $cm^2/(kV\ s)$.

I. Introduction

Capillary electrophoresis (CE) has proven to be powerful not only in the separation but also in the characterization of peptides and proteins. There are a very large number of CE options, for example, capillary micellar electrochromatography, capillary gel electrophoresis, free solution capillary electrophoresis (FSCE), and capillary isotacophoretic.[1] Among these, FSCE is best suited for theoretical study because the condition of free solution results in a relatively simple model system to examine the relation between mobility and chemico-physical properties, such as size and charge. In recent years, considerable work has been done in developing semiempirical models to predict the mobility of a peptide using peptide molecular weight, hydrodynamic radius, charge, and the number of amino acids in the peptide. Among the simplest models, the Offord model ($\mu = z_T/M^{2/3}$)[2] has been shown to give good correlations with a lot of experimental data,[3] where μ is the free solution electrophoretic mobility, z_T is the net charge, and M is the molecular weight. In the past few years, more sophisticated semiempirical computer models have been developed that take a more detailed account of peptide charge, composition, and the number of amino acids.[3−6] Under specific experimental conditions (pH, temperature, solvent, and buffer composition), these models can be very accurate. Our lab has taken a different approach by developing a purely structure-based methodology grounded on fundamental electrohydrodynamic theory.[7,8] Each amino acid is represented by two beads, one for the backbone of the peptide and one for the side group of the amino acid. The size and charge of each bead are fixed in a way that is entirely independent of electrophoretic mobility measurements, and this greatly limits the number of adjustable parameters available in modeling. However, the methodology developed previously is strictly valid for weakly charged peptides in which the beads are small compared to $1/\kappa$, where κ is the Debye−Huckel screening parameter. Specifically, only terms to first order in κa were retained, where a is a typical subunit radius used in modeling.[7] By "weakly charged", we mean the absolute surface or ζ potential does not exceed 25 mV[9] or, equivalently, the absolute electrophoretic mobility does not exceed approximately 0.20 $cm^2/(kV\ s)$.[10] For more highly charged macro-ions, ion relaxation needs to be taken into account. In the present work, ion relaxation refers to the perturbation of the ion atmosphere in the vicinity of the particle from its equilibrium distribution in response to the imposed electric and flow fields.[11−14]

In past work,[8] generally good agreement was obtained between model mobilities and experimental results[4] of 58 peptides ranging in size from 2 to 39 amino acids. For the most part, this particular set of peptides is weakly charged under the conditions of the experiment (pH = 2.5), and the salt concentration was low enough (35.3 mM monovalent salt) to ensure that κa is small. In the present work where ion relaxation and the restriction that $\kappa a \ll 1$ is relaxed are taken into account, all of the peptides studied previously are re-examined. We also examine a set of 24 peptides[3,5] which, as a group, tend to be more highly charged than the 58 peptides examined previously.[8] Because of this greater charge, this set is more prone to exhibit

* Corresponding author. E-mail: sallison@gsu.edu. Phone: 404-651-1986.

10.1021/jp065079u CCC: $33.50
Published on Web 11/21/2006

substantial ion relaxation effects. In addition, the "charge ladder" of human carbonic anhydrase is examined in which the charge of the protein, which remains in its native conformation, is varied over a wide range.[15] This example clearly shows how ion relaxation influences mobility as charge is varied. It also demonstrates that our procedure of correcting unrelaxed mobilities to account for ion relaxation is effective.

Including ion relaxation complicates the problem substantially because of the coupling of the fluid flow, ion densities, and external electric and/or flow fields.[11−14] In section III, the procedure used to account for the ion relaxation effect is described in detail. Briefly, we assume $\mu_r/\mu_{nr} = \mu_{rs}/\mu_{nrs}$ where μ_r/μ_{nr} is the ratio of peptide mobility with relaxation to that without relaxation and μ_{rs}/μ_{nrs} represents a similar ratio for spheres with the same hydrodynamic radius and average electrostatic surface potential and under the same solvent/salt/buffer conditions as our model peptide. The ratio of the spherical model particles is readily determined using the method of O'Brien and White.[14]

The outline of this paper is as follows: In section II, we outline the methodology used to determine unrelaxed mobilities, μ_{nr}, of model peptides and proteins. This includes a discussion of generating conformations from crystal structures in certain cases as well as the inclusion of finite bead size effects. Details regarding how finite bead size effects influence the calculation of electrostatic potential and mobility are given in Appendices A and B. In section III, the method used to account for ion relaxation is examined. In section IV, results are presented, first, on a set (set 1) of 50 peptides which tend to be weakly charged and, second, on how finite bead size effects and ion relaxation effects influence mobility. A similar analysis is then carried out on a smaller set (set 2) of more highly charged peptides where relaxation effects tend to be more significant. Finally, the protein charge ladder of human carbonic anhydrase is considered. This example clearly demonstrates the effect of ion relaxation on mobility as well as the effectiveness of our simple procedure in accounting for it. Section V summarizes the principle conclusions of the paper and briefly discusses future work.

II. Outline of the Methodology Used To Determine μ_{nr} for Peptides and Proteins

As discussed previously,[8] the peptide or protein which is made up of N amino acids is represented as $2N$ beads with 2 beads representing each amino acid. A principal motivation for choosing such a simple model is that computation time, which scales roughly as the number of beads squared (see, e.g., refs 16 and 17), is greatly reduced. As an illustrative example, a mobility calculation of a single conformation of a flexible model macromolecule consisting of 240 plates using a full boundary element (BE) procedure required 2 days of single processor time on a Silicon Graphics workstation (see ref 16, p 2565). By comparison, a mobility calculation of a flexible peptide consisting of 84 beads and involving 100 independent conformations using the present methodology required only 20 min under similar computing conditions.

In this bead model, the radius of the "backbone" bead is chosen to correspond to half the average distance between successive α carbons, 0.19 nm. The radius of the "side" bead is chosen to reproduce the translational diffusion constant of the specific amino acid. Transport rather than structural considerations is used to parametrize the side beads. We believe that this is appropriate since the physical quantity of interest in the present work is a translational transport property, the electrophoretic mobility. Specfic values for the radii of the side beads of different amino acids are given in Table 1 of reference 8. For peptides that are assumed to be unfolded, conformations are generated using the Flory rotation matrix approach[18] as discussed previously.[8] Typically, 100 conformations are randomly generated, and an average μ is computed from this ensemble. In certain cases, we also consider conformations derived from the crystal structure or Protein Data Bank coordinate file when available. This crystal structure approach is described in the next paragraph. Although the bead model used in this work is lacking in atomic detail, it should be sufficiently realistic to mimic global conformation and yield fairly accurate translational transport properties such as translational diffusion constants and electrophoretic mobilities. For other transport properties such as rotational diffusion constants and intrinsic viscosities, models that account more accurately for the actual surface of hydrodynamic shear should be used.[17,19]

In the crystal structure approach, the backbone beads are placed at the crystallographic coordinates of the α carbons. Let $\mathbf{r}_j$ denote the virtual bond vector extending from the α carbon of the jth amino acid to the α carbon of the $j + 1$ amino acid. Also let $\mathbf{r}_0$ extend from the N of the N-terminus to the first α carbon, and let $\mathbf{r}_N$ extend from the Nth α carbon to the C of the C-terminus. The side beads are initially placed along the vector extending from the α carbon to the β carbon of the side group. The distance of the center of the side bead from the center of the backbone bead is set to the sum of the radii of the two beads. In the event the jth amino acid is glycine, which has no β carbon, the side bead is initially placed along the vector $-(\mathbf{r}_{j-1} + \mathbf{r}_j)$. These positions may have to be modified to avoid bead overlap. If the backbone beads overlap, which occurs if the distance between successive α carbons falls below 0.38 nm, then the radii of the two backbone beads are shrunk by an equal amount to ensure that the beads are just touching. The corresponding distances of side beads from their associated backbone beads are also adjusted to ensure that the side beads and their associated backbone beads just touch. No further adjustment is made regarding the positions or radii of the backbone beads. For the side beads, every interbead distance is checked for possible overlap. If overlap occurs, a new possible position is chosen completely at random, subject to the constraint that the side bead just touches its corresponding backbone bead. If the new position still overlaps another bead, then the position is rejected and the procedure is repeated. If a suitable position is not found after 100 attempts, then the radius of the side bead is reduced by 10% and the above procedure is repeated. When a suitable position for a side bead is found, the same procedure is applied to successive side beads until a complete peptide structure is generated.

With regard to the macro-ion model itself, past work has shown that μ depends primarily on net charge and global structure.[8,10,20] Local structural features or subtle variations in the charge distribution have little effect on μ. At the same time, however, it is important that the beads making up the model structure do not overlap. The procedure described in the previous paragraph yields structures that both preserve overall conformation and ensure bead overlap does not occur.

In addition to conformation, the assignment of charge to the ionizable residues making up the peptide is of fundamental importance. If the pH of the solution and the pK_a of a particular residue are known, then it is straightforward to calculate the charge state of that residue. It is well-known, however, that environmental influences cause the pK_a of a particular residue to be different from that of the free amino acid.[21] In particular, the charge state of the neighborhood of a specific residue will

influence its pK_a, and this can be approximated in terms of simple electrostatic and free energy arguments.[8,10,22,23] The procedure employed in the present work to deal with this problem has been discussed previously.[8]

At this point, we have a model structure and have assigned charges. The next step is determining the electrophoretic mobility, μ, which also requires knowledge of the equilibrium electrostatic potential, $\Lambda(\mathbf{y})$, at position $\mathbf{y}$ in the vicinity of our model macro-ion. It is assumed that our macro-ion, modeled as a bead array, is weakly charged. Hence, the linear Poisson−Boltzmann equation must be solved to determine $\Lambda(\mathbf{y})$. We do, however, want to account for the finite size of the beads and exclude salt from the interior of the beads. Thus, our model is not limited to the restriction $\kappa a \ll 1$ where κ is the Debye−Huckel screening parameter given by eq A18. A detailed derivation of $\Lambda(\mathbf{y})$ is given in Appendix A, and the key results are summarized by eqs A26−28.

Previously,[8] we described in detail a procedure for calculating μ under the condition $\kappa a \ll 1$. In the present work, this is relaxed. A detailed derivation is given in Appendix B, and the key equations are B39 for μ and B48 for the reduced hydrodynamic forces on the individual beads. To summarize, the equilibrium electrostatic potential is solved at the level of the linear Poisson−Boltzmann equation, and unrelaxed mobilities, μ_{nr}, are computed for model structures. As in previous work,[7,8] hydrodynamic interaction is orientationally pre-averaged. Also, the internal field effect is ignored. These assumptions/approximations are believed to yield mobilities that are accurate to within a few percent.[7]

III. Inclusion of Ion Relaxation

The relaxation correction, C, is defined

$$C = \frac{\mu_r}{\mu_{nr}} \tag{1}$$

where μ_{nr} and μ_r are the mobilities of a particular model particle in the absence and presence of ion relaxation. Also, let R denote the hydrodynamic radius of the model particle, which is defined in terms of its translational diffusion constant D_T,

$$R = \frac{k_B T}{6\pi\eta D_T} \tag{2}$$

where k_B is Boltzmann's constant, T is absolute temperature, and η is solvent viscosity. For a model structure, D_T is computed using long established procedures.[24,25] In previous work,[26] it was shown that C for a prolate ellipsoid and C for a sphere with the same R are nearly identical under conditions of the same solvent temperature, salt concentration and composition, and ζ (average electrostatic surface) potential. It should be emphasized that this is independent of the axial ratio of the ellipsoid. Consequently, we shall simply assume that C for an arbitrary irregular structure is equal to that of an equivalent sphere.

$$C \cong \frac{\mu_{rs}}{\mu_{nrs}} \tag{3}$$

The advantage of eq 3 is that relaxed and unrelaxed mobilities of spheres are relatively easy to determine using available procedures.[14] The reduced potential, y, is defined

$$y = \frac{q\langle\Lambda\rangle}{k_B T} \tag{4}$$

where $\langle\Lambda\rangle$ represents the electrostatic potential averaged over the surface of the model particle (ζ potential). On physical grounds, C varies continuously as y varies and has its maximum value of 1.0 at $y = 0$. This is because ion relaxation always acts to reduce the absolute electrophoretic mobility and vanishes in the limit of zero ζ potential. Also, $dC/dy = 0.0$ at $y = 0$. At small $|y|$, we can write

$$C \cong 1 + a_1 y^2 + a_2 y^3 + a_3 y^4 \tag{5}$$

The a_j coefficients in eq 5 will depend on salt concentration, ion type, and R. All of the peptide mobility measurements (but not the protein charge ladder results[15]) reported in this work were carried out in 35.3 mM $Na^+HPO_4^-$ buffer at pH = 2.5 and 22 °C.[4,5] We examined model spheres of variable y in the size range 0.5 nm ≤ R ≤ 2.0 nm and obtained the following coefficients in this particular salt/buffer system (R is in nanometers).

$$a_1 = -0.005 - 0.021R \tag{6a}$$

$$a_2 = -0.0021 + 0.0024R \tag{6b}$$

$$a_3 = +0.000\,13 + 0.000\,08R \tag{6c}$$

Once the hydrodynamic radius of a peptide and y are determined, eqs 6a−c can be used to estimate C. Once the unrelaxed mobility, μ_{nr}, is determined, the relaxed mobility is simply $\mu_r = C\mu_{nr}$.

For the charge ladder of human carbonic anhydrase,[15] the temperature was 25 °C, pH = 8.4, and the salt consisted of 7.9 mM $Tris^+glycine^-$. Under these conditions,

$$a_1 = -0.0152 - 0.0066R \tag{7a}$$

$$a_2 = -0.0006 + 0.0003R \tag{7b}$$

$$a_3 = +0.000\,11 + 0.0001R \tag{7c}$$

It is important to emphasize that these coefficients depend strongly on ionic strength as well as the specific ion composition of the buffer.

Since peptides are irregularly shaped, it can be argued that the relaxation correction may be more complicated than that of axisymmetric prolate ellipsoids. As a preliminary consideration of this issue, we shall first consider the case of hen eggwhite lysozyme that was studied by a BE procedure using an atomically detailed surface model derived from the crystal structure of the protein.[27] This protein has a hydrodynamic radius of 2.02 nm, and at 0 °C in 0.15 M NaCl at pH = 3, the average reduced surface potential, y, is approximately 1.35. From BE modeling, the ratio μ_r/μ_{nr} under these conditions is 0.952 (see Figure 6 of ref 27). The corresponding ratio using spheres is 0.956. Consequently, the simple procedure used to account for the relaxation effect is quite accurate but not exact in this particular case. Nonetheless, the correction does succeed in properly accounting for much of the effect. A more complete analysis of the accuracy of the relaxation correction is given at the end of the next section by the example of the charge ladder of human carbonic anhydrase.

IV. Results and Discussion

To check the accuracy of the more general methodology discussed in sections II and III as well as to determine the

TABLE 1: Transport Properties of Set 1 (50 Peptides)

peptide	sequence	z_T	μ_{exp}	$\mu_{nr}{}^a$	$\mu_{nr}{}^b$	$\mu_r{}^c$
1	DD	0.694	0.103	0.121	0.122	0.120
2	FD	0.773	0.130	0.119	0.121	0.119
3	EE	0.769	0.125	0.118	0.120	0.118
4	GG	0.818	0.217	0.204	0.205	0.197
5	AA	0.818	0.193	0.172	0.174	0.168
6	PG	0.818	0.184	0.181	0.182	0.176
7	VV	0.817	0.154	0.122	0.124	0.122
8	FG	0.818	0.152	0.143	0.145	0.142
9	FA	0.817	0.149	0.136	0.138	0.135
10	FV	0.817	0.139	0.118	0.120	0.118
11	MM	0.817	0.139	0.140	0.142	0.139
12	YY	0.817	0.121	0.108	0.111	0.109
13	AAA	0.888	0.154	0.152	0.154	0.150
14	SSS	0.884	0.132	0.146	0.148	0.144
15	AAAA	0.913	0.139	0.133	0.135	0.132
16	AAAAA	0.921	0.123	0.120	0.122	0.120
17	YGGFM	0.921	0.095	0.094	0.096	0.095
18	RPPGF	1.888	0.184	0.199	0.203	0.193
19	AAGIGILTV	0.936	0.065	0.073	0.076	0.075
20	YMDGTMSQV	0.882	0.060	0.062	0.064	0.063
21	VLQELNVTV	0.918	0.066	0.061	0.063	0.063
22	RPPGFSPFR	2.777	0.197	0.207	0.213	0.200
23	AFLPWHRLF	2.831	0.166	0.191	0.196	0.184
24	VISNDVCAQV	0.895	0.058	0.059	0.061	0.061
25	KLVVVGADGV	1.882	0.131	0.128	0.132	0.128
26	KLVVVGAAGV	1.923	0.141	0.133	0.137	0.133
27	NSFCMGGMNRR	2.718	0.183	0.182	0.184	0.178
28	RPKPQQFFGLM	2.904	0.170	0.182	0.189	0.178
29	ACLGRDRRTEE	3.602	0.210	0.230	0.235	0.213
30	DAEKSDICTDEY	1.644	0.099	0.099	0.101	0.100
31	TTIHYNYICNSS	1.926	0.106	0.115	0.118	0.115
32	PHRERCSDSDGL-ace	2.739	0.195	0.173	0.176	0.167
33	ACPGTDRRTGGGN	2.796	0.151	0.182	0.186	0.175
34	ACPGKDRRTGGGN	3.717	0.191	0.239	0.243	0.219
35	MGGMNWRPILTIIT	1.926	0.102	0.109	0.112	0.110
36	SPALNKMFCELAKT	2.838	0.157	0.161	0.166	0.159
37	HMTEVVRHCPHHER	6.323	0.264	0.335	0.344	0.279
38	LAKTCPVRLWVDSTPP	2.857	0.151	0.146	0.15	0.144
39	LGRNSFEVCVCACPGRD	2.81	0.137	0.142	0.148	0.143
40	KLVVVGAGDVGKSALTI	2.855	0.137	0.139	0.144	0.139
41	TPPPGTRVQQSQHMTEV	2.878	0.142	0.139	0.143	0.137
42	YKLVVVGAAGVGKSALT	2.903	0.142	0.142	0.147	0.141
43	YGLVVVGACGVGKSALT	2.907	0.143	0.140	0.146	0.140
44	YNYMCNSSGMGGMNRRP	2.824	0.143	0.143	0.148	0.143
45	YKLVVVGAVGVGKSALT	2.903	0.151	0.139	0.144	0.138
46	YKLVVVGARGVGKSALT	3.883	0.178	0.185	0.191	0.178
47	PPPGTRVRVMAIYKQSQ	3.887	0.182	0.185	0.191	0.177
48	DGLAPPQHRIRVEGNLR	4.496	0.195	0.222	0.227	0.205
49	VPYEPPEVGSVYHHPLQLHV	3.753	0.153	0.157	0.161	0.152
50	HQIINMWQEVGKAMYAPPISGQIRRIHIGPGRAFYTTKN	7.762	0.175	0.206	0.213	0.189

[a] Finite bead size effects not included and no relaxation correction. [b] Finite bead size effects included, but no relaxation correction. [c] Finite bead size effects included plus ion relaxation.

improvement on unrelaxed mobilities by taking a more detailed account of the finite size of the model beads, we have examined two sets of peptides where experimental data is available. The first set of 50 consists of peptides ranging in size from 2 to 39 amino acids that, for the most part, are weakly charged.[4] Consequently, neglect of ion relaxation should be a good approximation for many of the peptides in this set. The second set of 24 peptides ranges in size from 2 to 42 residues, and these tend to be more highly charged than the first set.[5] The second set serves as a more stringent test of our procedure to account for ion relaxation than the first set. In addition, other investigators[6] have analyzed this second set in terms of several different semiempirical models that shall be discussed. The actual experiments[4,5] were carried out at 22 °C in a buffer system consisting of 50 mM phosphoric acid that was adjusted to pH 2.5 with triethylamine. At this pH, the peptides are expected to be largely unfolded. Using a $pK_a = 2.12$ for the first acid dissociation constant of phosphoric acid, we estimate the ion strength, I, to be 35.3 mM, which also equals the concentration of $H_2PO_4^-$. The solvent dielectric constant and solvent viscosity, η, are taken to be 80 and 0.955 cP, respectively. The Debye−Huckel screening parameter, κ, equals 0.622 nm^{-1} under the conditions of the experiment.

Shown in Tables 1 and 2 are the sequences, experimental mobilities, μ_{exp}, and three different model mobilities for these two sets of peptides. The first model mobilities listed, $\mu_{nr}{}^a$ (footnote *a*), ignore ion relaxation and assume $\kappa a \ll 1$ (where a is a typical bead size). The second set of model mobilities, $\mu_{nr}{}^b$ (footnote *b*), relax this approximation. It is clear from both tables that taking a more accurate account of the finite size of the model subunits produces a change in model mobility of approximately 1%. Under the conditions of the experiment and when a typical bead radius of 0.25 nm is taken, $\kappa a = 0.16$; the "small bead approximation" is a reasonable assumption. We

TABLE 2: Transport Properties of Set 2 (24 Peptides)

peptide	sequence	z_T	μ_{exp}	$\mu_{nr}{}^a$	$\mu_{nr}{}^b$	$\mu_r{}^c$
1	FF	0.817	0.128	0.113	0.115	0.113
2	FL	0.817	0.133	0.12	0.123	0.120
3	LL	0.817	0.146	0.128	0.131	0.128
4	WW	0.817	0.110	0.111	0.114	0.112
5	FFF	0.886	0.104	0.097	0.0998	0.0982
6	KKKK	4.380	0.330	0.43	0.439	0.341
7	KKKKK	5.315	0.330	0.461	0.472	0.346
8	YGGFL	0.918	0.0975	0.091	0.0934	0.0921
9	ACHGRDRRT	4.467	0.265	0.33	0.336	0.285
10	VVRRYPHHE	4.628	0.274	0.307	0.315	0.265
11	CRHRRRHRRGC	8.480	0.297	0.532	0.546	0.317
12	CRHHRRRHRRGC	9.456	0.297	0.559	0.573	0.309
13	HMTEVRRYPHHER	6.290	0.264	0.342	0.351	0.282
14	HMTEVRHCPHHER	6.287	0.264	0.355	0.363	0.290
15	HRSCRRRKRRSCRHR	11.20	0.303	0.562	0.579	0.310
16	RTHCQSHYRRRHCSR	8.423	0.290	0.427	0.440	0.306
17	YAEDGVHATSKPARR	4.441	0.214	0.241	0.247	0.224
18	VVRRCPHQRCSDSGL	4.734	0.208	0.236	0.241	0.212
19	DGLAPPQHRIRVFGNLR	4.532	0.190	0.223	0.228	0.206
20	NHQLLSPAKTGWRIFHP	4.772	0.194	0.231	0.239	0.216
21	RTHGQSHYRRRHCSRRRLHRIHRRQ	15.29	0.290	0.532	0.543	0.262
22	FLTPKKLQCVDLHVISNDVCAQVHPQKVTK	6.478	0.187	0.202	0.209	0.189
23	KQIINMWQEVGKAMYAPPISGQIRRIHIGPGRAFYTTKN	7.775	0.178	0.204	0.209	0.186
24	DRVIEVVQGAYRAIRHIPRRIRGQLERRIHIGPGRAFYTTKN	12.17	0.208	0.295	0.292	0.218

[a] Finite bead size effects not included and no relaxation correction. [b] Finite bead size effects included, but no relaxation correction. [c] Finite bead size effects included plus ion relaxation.

now turn to the effect of including ion relaxation in the model calculations and the overall accuracy of the model mobilities. We define the relative error, E,

$$E = \frac{\mu_{exp} - \mu_{mod}}{\mu_{exp}} \tag{8}$$

where μ_{mod} is a model mobility in the absence (μ_{nr}) or presence (μ_r) of ion relaxation. In the present analysis, we shall focus on the modeling that includes finite bead size correction. For set 1, $\langle E_{nr}\rangle = -0.041$, $\langle E_{nr}{}^2\rangle^{1/2} = 0.110$, $\langle E_r\rangle = 0.0039$, and $\langle E_r{}^2\rangle^{1/2} = 0.080$. The brackets indicate an average over all of the peptides in the data set. The negative value of $\langle E_{nr}\rangle$ is due to the fact that ion relaxation, present in an actual experiment, produces absolute mobilities that are lower than they would be in the absence of ion relaxation. On average, including ion relaxation brings model and experimental mobilities into better agreement. For the set 1 peptides, model (with relaxation) and experimental mobilities, on average, agree to better than 1%. The low value of $\langle E_r\rangle$ indicates there are no significant systematic errors in our modeling. This, in turn, suggests that our modeling captures the essential physics of the phenomenon of electrophoresis.

Nonetheless, substantial discrepancies do persist for particular peptides, as evidenced by the fairly large $\langle E^2\rangle^{1/2}$ values. As discussed previously,[8] this is probably due to errors in estimating the charge of the peptides in specific cases. Error in estimating charge in specific cases, which could be due to underestimating or overestimating the pK_a of specific residues, could very well be responsible for the "scatter" seen in a comparison of μ_{exptl} and μ_r. The importance of including ion relaxation is made even more evident by set 2, where the peptides tend to be more highly charged than those in set 1. For set 2, $\langle E_{nr}\rangle = -0.294$, $\langle E_{nr}{}^2\rangle^{1/2} = 0.430$, $\langle E_r\rangle = -0.013$, and $\langle E_r{}^2\rangle^{1/2} = 0.069$. Not surprisingly, neglect of ion relaxation produces an even greater error for this set of peptides, including ion relaxation results in an overall accuracy that is comparable to that of set 1. Plotted in Figure 1 are E_{nr} and E_r for all 74 peptides versus the net charge-to-size ratio, Z/N. As Z/N increases and the effects of ion relaxation on mobility increase, E_{nr} tends to deviate more strongly from 0 as expected. It is worth noting that, for E_r, the greatest scatter occurs at low Z/N. This can be explained as follows. When the net absolute charge, $|Z|$, of the peptide is low, a small absolute error in estimating Z can produce a large relative error in Z and hence E. Thus, inaccuracy in estimating peptide charge is likely to be a principal cause of error in predicting peptide mobilities. On the basis of Figure 2, this error is about 12% in the worst cases. The random scatter seen argues against systematic error in our modeling procedure. Another possible source of error involves inaccurate sampling of peptide conformations. In previous work,[8] mobility was shown to depend on conformation, but that dependence is fairly weak. The mobility of the pentapeptide, AAAAA, was shown to vary from 0.111 (fully extended) to 0.125 (compact) in a study of 5000 independent conformations. If a peptide was trapped in a single conformation (fully compact, e.g., with $\mu = 0.125$ cm^2/(kV s)), it is conceivable that a predicted mobility based on conformations selected at random (giving $\langle\mu\rangle = 0.119$ cm^2/(kV s) in the above example) would produce error (5% in the above example).

Other investigators have developed sophisticated semiempirical models that can be quite accurate for peptides under specific conditions. These include the multivariable (MV) model of Janini and co-workers[5] and the multiple linear regression (MLR) and artificial neural network (ANN) methods. The latter two methods were developed by Jalali-Heravi and co-workers.[6] Listed in Table 3, along with experimental mobilities, are the corresponding bead method mobilities of the present work as well as predicted MV, MLR, and ANN mobilities. Plotted in Figure 2 are the corresponding E values for the four models. (Values for the bead model in the absence of the ion relaxation correction are not included.) The corresponding $\langle E^2\rangle^{1/2}$ values are 0.069 (bead model with relaxation correction), 0.045 (MV), 0.118 (MLR), and 0.058 (ANN). Although the bead model is not better than the semiempirical models, it is competitive with all of them. Furthermore, there is a considerable advantage to a structure-based model grounded in fundamental electrokinetic theory as discussed in Conclusions.

Although not as accurate as the semiempirical methods discussed in the previous paragraph, a simple and effective way

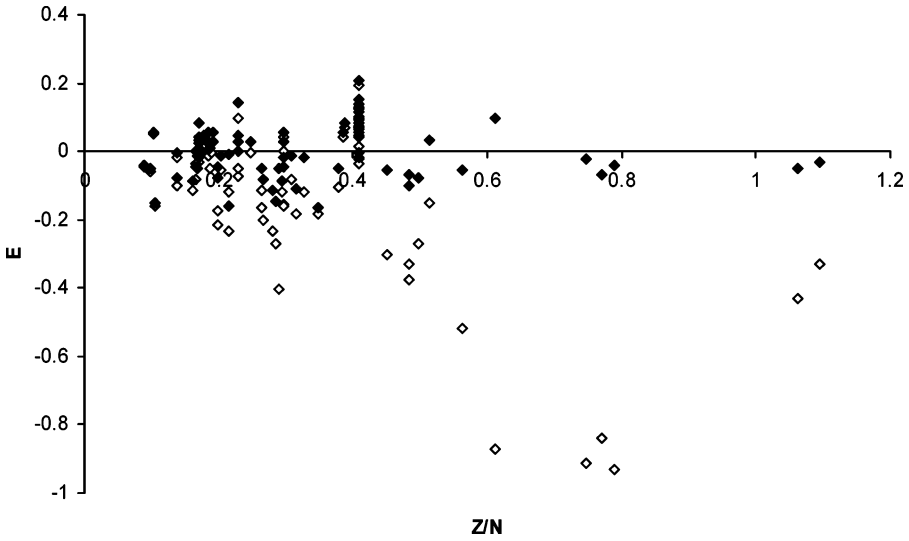

Figure 1. *E* versus *Z*/*N* for model mobilities. Results of 74 peptides (sets 1 and 2) are included. Unfilled and filled diamonds correspond to model mobilities without and with the ion relaxation correction, respectively.

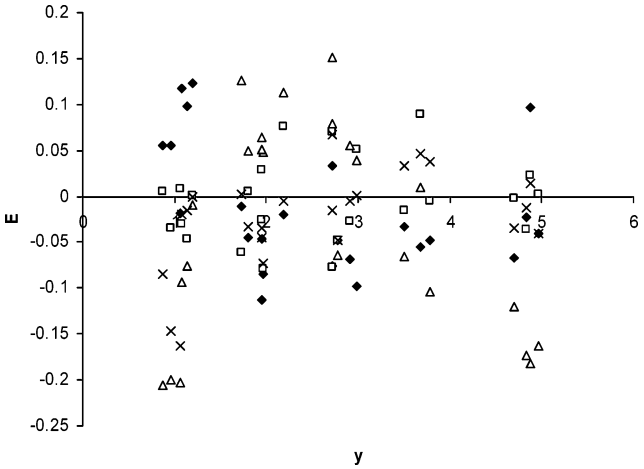

Figure 2. Comparison of several models with experiment versus *y*. Results are for peptide set 2. Bead model with ion relaxation (diamonds), MV (squares), MLR (triangles), and ANN (crosses).

used by numerous investigators over the last 20 years of relating mobility to net charge, *Z*, and peptide molecular weight, *M*, has been to simply write[4,28−36]

$$\mu = AZ/M^{\alpha} \tag{9}$$

where *A* and α are empirical constants. Typically, $\alpha \cong 2/3$ under most conditions. Equation 9 can be rearranged to give

$$-\ln\left(\frac{\mu}{Z}\right) = -\ln(A) + \alpha \ln(M) \tag{10}$$

This is plotted in Figure 3 for all 74 peptides (sets 1 and 2) listed in Tables 1 and 2. Experimental points are indicated by filled squares. Model results without and with the ion relaxation correction are indicated by unfilled diamonds and squares, respectively. As can be seen, there is considerable scatter in the results. Plotted in this way, model results without ion relaxation always lie below those with ion relaxation. More highly charged peptides tend to lie above their more weakly charged counterparts. It is this factor which is closely tied to the relaxation correction that is responsible for the scatter seen in the figure.

Next, we shall consider the case of a protein charge ladder.[15] The reason for presenting this analysis is to address two issues.

TABLE 3: Comparison of Different Models with Experiment (Peptide Set 2)

no.	*y*	μ(expt)[a]	μ(BM)[c]	μ(BM)[d]	μ(MV)[a]	μ(MLR)[b]	μ(ANN)[b]
1	1.072	0.128	0.115	0.113	0.1318	0.1399	0.1306
2	1.135	0.133	0.123	0.120	0.1391	0.143	0.1351
3	1.194	0.146	0.131	0.128	0.1458	0.1473	0.1461
4	1.064	0.11	0.114	0.112	0.1091	0.1323	0.128
5	0.967	0.104	0.0998	0.0982	0.1076	0.1248	0.1192
6	3.509	0.33	0.439	0.341	0.3353	0.3517	0.3188
7	3.784	0.33	0.472	0.346	0.3318	0.3645	0.3176
8	0.867	0.0975	0.0934	0.0921	0.097	0.1176	0.1058
9	2.717	0.265	0.336	0.285	0.2854	0.2439	0.269
10	2.712	0.274	0.315	0.265	0.2546	0.2324	0.2555
11	4.693	0.297	0.546	0.317	0.2975	0.3325	0.3072
12	4.960	0.297	0.573	0.309	0.2961	0.3454	0.3089
13	2.918	0.264	0.351	0.282	0.2711	0.2492	0.2654
14	2.984	0.264	0.363	0.290	0.2507	0.2535	0.2636
15	4.826	0.303	0.579	0.310	0.3141	0.3557	0.3068
16	3.684	0.29	0.440	0.306	0.2639	0.2872	0.2764
17	1.946	0.214	0.247	0.224	0.2194	0.2004	0.2215
18	2.188	0.208	0.241	0.212	0.1922	0.1844	0.2092
19	1.959	0.19	0.228	0.206	0.2049	0.181	0.204
20	1.949	0.194	0.239	0.216	0.1885	0.184	0.2028
21	4.872	0.29	0.543	0.262	0.2832	0.3429	0.2857
22	1.736	0.187	0.209	0.189	0.1983	0.1635	0.1865
23	1.796	0.178	0.209	0.186	0.1771	0.1691	0.1839
24	2.782	0.208	0.292	0.218	0.2179	0.2213	0.218

[a] Data comes from ref 5. [b] Data comes from ref 33. [c] Bead model without ion relaxation. [d] Bead model with ion relaxation.

First, it shows that the relaxation correction works well for globular proteins. Second, the simple bead models used in the present work yield electrophoretic mobilities that are comparable to those using BE modeling that accounts more accurately for the actual surface of hydrodynamic shear. Protein charge ladders are collections of protein derivatives where the number of charge groups is varied by partial acylation of lysine residues or by amidation of glutamic and aspartic acid residues.[10,15,23] Modified proteins which have the same number of acylated sites have approximately the same charge and migrate with approximately the same mobility. In this work, we consider the example human carbonic anhydrase II.[15] The charge ladder was formed by partial acylation of a variable number of the 23 lysines present in the protein. For modeling, bead coordinates were generated from the crystal structure available through the Protein Data Bank (PDB code 1CA2). It was assumed that the conformation of the protein remains unchanged as it is acylated. To examine, in a systematic manner, the importance of ion relaxation, mobilities

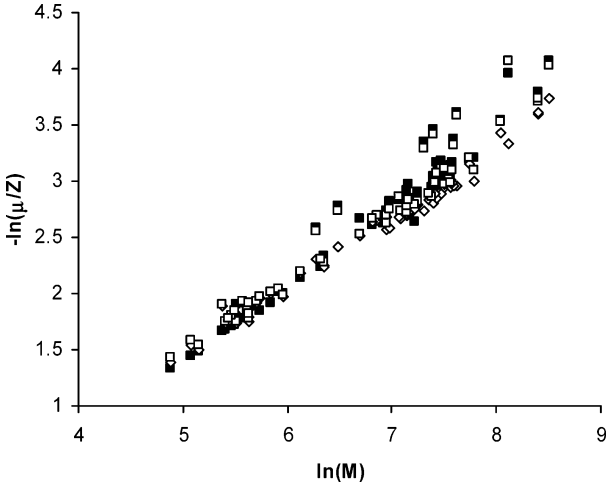

Figure 3. Correlation of experimental and model mobilities with net charge, *Z*, and molecular weight, *M*. Results of 74 peptides (sets 1 and 2) are included. Experimental data points are represented by filled squares. Model results without and with the ion relaxation correction are indicated by unfilled diamonds and squares, respectively.

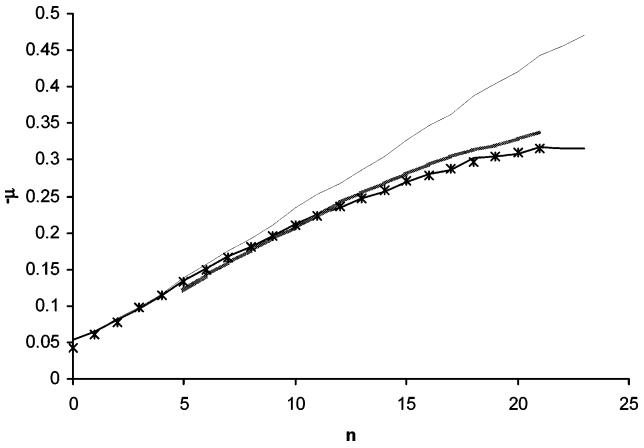

Figure 4. Mobilities versus *n* for human carbonic anhydrase II. The studies come from ref 15 and were carried out in 25 mM Tris base plus 192 mM glycine at 25 °C and pH = 8.4. BE model including ion relaxation[10] is represented by the shaded line, μ_{nr} is represented by a thin solid line, μ_r is represented by a thick solid line, and experimental mobilities are represented by asterisks.

are plotted versus the number of modified lysine residues (*n*). The unmodified protein is negatively charged, and as *n* increases, the net absolute charge of the protein increases. Figure 4 summarizes the principal results. Experimental results are indicated with asterisks, and bead model results without and with the relaxation correction are indicated with weak and heavy solid lines, respectively. As *n* increases, the absolute charge of the protein increases and ion relaxation becomes progressively more important. From this example, it is clear that ion relaxation becomes important when $|\mu|$ exceeds approximately 0.2 cm^2/(kV s). The good agreement between modeling (with ion relaxation) and experimental results confirms the accuracy of the bead methodology in a situation quite different from the peptides considered previously. Also included in Figure 4 are results from an earlier BE modeling study[10] indicated by the thick, shaded line. In BE modeling, the macro-ion is modeled as an irregularly shaped rigid body with charges distributed within.[10,37] Also, ion relaxation is included in this case, and its inclusion is determined by a direct numerical solution of the coupled electrokinetic field equations.[37−39] Although the BE results are expected to be accurate, they also require much more computation time than the bead model results of the present study. It is worth noting that the bead model results are in about as good of an agreement with experimental results as the earlier BE modeling results.

V. Conclusions

The bead methodology, initially developed in previous work,[8] differs from semiempirical approaches[5,6] in three significant ways. First, it is structure-based. Second, it is formally grounded in electrokinetic theory. Third, its parametrization is totally independent of mobility measurements. Consequently, it can be applied to a broad range of flexible biomolecules under a wide range of experimental conditions, and it can potentially be used to extract charge and structural information. The principal objectives of the present study involve the analysis of two assumptions of our earlier work and generalizing the methodology to deal with them. These two assumptions and how they impact present and future work are summarized below.

First, the restriction that $\kappa a \ll 1$ (where κ is the Debye−Huckel screening parameter and *a* is a typical subunit radius in our model) has been removed. For the peptides under the conditions examined in this paper, $\kappa a \cong 0.16$, and the assumption of a small κa is shown to yield accurate mobilities. It should be emphasized, however, that this is specific to the system of interest. For peptides, for example, the assumption becomes progressively worse as the salt concentration increases. For another example, suppose we wish to model duplex DNA as a semiflexible string of touching beads with radii of 1.59 nm.[40] In this case, $\kappa a \cong 0.58$ in a monovalent salt solution of 20 mM at room temperature, and finite bead effects can be expected to be much more significant than they are in the peptide systems examined in the present work. This is a subject under investigation in our laboratory at the present time.

Second, the effect of ion relaxation is accounted for in the present study. Ion relaxation becomes important when the local charge density becomes large. Provided the absolute elctrophoretic mobility of a peptide does not exceed approximately 0.2 cm^2/(kV s), ion relaxation can be ignored.[9,10] The direct inclusion of ion relaxation in electrophoresis theory is challenging because of the coupling of the electrodynamic, fluid flow, and ion transport field equations.[11−14,37−39] The approach used here is much simpler and is based on the observation that the relaxation effect is similar for irregularly shaped particles and spheres under similar conditions.[26] Thus, mobilities that do not account for ion relaxation are corrected using a correction factor derived from mobility studies of spheres under similar conditions. It should be emphasized that this approach is approximate and may not work well for highly asymmetrical particles. Also, the equilibrium potential is calculated at the level of the linearized Poisson−Boltzmann equation in this work. When the charge on the macro-ion is high, the nonlinear Poisson−Boltzmann equation should really be solved, and this will influence the relaxation correction. We have tested the algorithm by applying it to two sets of peptides (74 total) from the work of Janini and co-workers.[4,5] Some of the peptides in this data set are highly charged, and ion relaxation is predicted to have an effect on their mobilities. The model mobilities are in good agreement with experimental results when corrected for ion relaxation. It is also shown that the accuracy of the bead model methodology is competitive with the semiempirical methods developed by a number of investigators. As a final application, the bead model methodology is applied to the charge ladder of human carbonic anhydrase II.[15] In this example, the charge on the protein is varied in a systematic way, and protein

conformation does not change significantly as the charge is varied. When the charge of the protein is low, it is demonstrated that ion relaxation has little effect on mobility. When the charge is large, however, ion relaxation is important in reducing the absolute mobility relative to the "no relaxation" value. When corrected for ion relaxation, model and experimental mobilities are found to be in excellent agreement.

In the future, we plan to extend this work in several directions. First of all, we are now in a position to study other biomolecules such as single stranded DNA, RNA, and duplex DNA. These tend to be more highly charged than peptides, and thus, the relaxation effect is expected to be significant. Also, the model building blocks for these systems[40] will be larger than those for peptides making it more important to account for the finite size of the model subunits. Another assumption shall also be addressed in future work, and that is the assumption of pre-averaging the hydrodynamic interaction.[41] This assumption has been extensively analyzed by a number of investigators[42−45] with regard to nonelectrophoretic transport properties such as translational and rotational diffusion as well as intrinsic viscosity. This approximation is quite inaccurate for rotational diffusion and intrinsic viscosity[45] but works much better for translational diffusion where its use results in overestimating the diffusion constants by 0 to 8.3% depending on the structure involved. For electrophoretic mobility, the pre-averaging approximation is expected to work about as well as or perhaps better than it does for translational diffusion.[7] However, no systematic study of the pre-averaging approximation with regard to electrophoretic mobility has been carried out. Such a study is currently underway in our laboratory and shall be reported in the near future.

Appendix A: Equilibrium Electrostatics

Consider an array of N beads, not necessarily of equal size and charge, immersed in a fluid medium of dielectric constant ϵ_w. Let a_k and z_k denote the radius and charge (in protonic units) of bead k. It is assumed that the charge of each bead resides on the bead surface and that the bead surface is a conductor. Consequently, the electrostatic potential on the surface of bead k, ζ_k, is uniform. The fluid contains ions (from disassociated salt) of ambient concentration, c_{k0}, and valence, z_k'. In the framework of the continuum-primitive model, the electrostatic potential, $\Lambda(\mathbf{x})$, at position $\mathbf{x}$ in the fluid domain, obeys the Poisson−Boltzmann equation

$$\nabla^2\Lambda(\underline{x}) = -\frac{Cq}{\epsilon_w}\sum_k c_{k0} z_k' \exp(-\beta q z_k' \Lambda(\underline{x})) \qquad \text{(A1)}$$

where $C = 4\pi$ (in centimeter−gram−second units) or $1/\epsilon_0$ where ϵ_0 is the permitivity of free space (in meter−kilogram−second units), q is the protonic charge, and $\beta = 1/k_B T$ where k_B is Boltzmann's constant and T is absolute temperature. The sum in eq A1 extends over all of the ion species present in solution. The electrostatic boundary condition on the bead surface is

$$\epsilon_w p^e(\underline{x}_s) = \epsilon_w(\underline{\nabla}\Lambda(\underline{x}_s)\cdot\underline{\mathbf{n}}(\underline{x}_s))_{ext} = -C\sigma(\underline{x}) \qquad \text{(A2)}$$

where $\mathbf{x}_s$ is a point on the surface of a particular bead, $\mathbf{n}$ is the outward unit normal vector to the surface at that point, the "ext" subscript denotes the gradient is taken in the fluid domain adjacent to $\mathbf{x}_s$, and σ is the surface charge density on the bead.

In the present work, it is convenient to solve for Λ using the BE method.[46,47] The potential can be written

$$\Lambda(\underline{y})\,\Phi(\underline{y},V_e) = -\int_{V_e} F(\alpha,r)\,h(\alpha,\underline{x})\,dV_x - \sum_{k=1}^{N}\left[\int_{S_k}[F(\alpha,r)\,p^e(x) - \zeta_k F'\alpha,r)]\,dS_x \right. \qquad \text{(A3)}$$

where V_e is the fluid domain (exterior to the volume occupied by the beads themselves), $r = |\mathbf{x} - \mathbf{y}|$, and

$$F(\alpha,r) = \frac{e^{-\alpha r}}{4\pi r} \qquad \text{(A4)}$$

where α is an arbitrary real and positive constant,

$$h(\alpha,\underline{x}) = \nabla^2\Lambda(\underline{x}) - \alpha^2\Lambda(\underline{x}) \qquad \text{(A5)}$$

$$F'(\alpha,r) = \underline{\nabla}_x F(\alpha,r)\cdot\underline{n}(\underline{x}) \qquad \text{(A6)}$$

Also, $\Phi(\mathbf{y},V_e)$ equals 1 if $\mathbf{y}$ lies in V_e, equals 0 if $\mathbf{y}$ lies outside of V_e, and equals 1/2 if $\mathbf{y}$ lies on the surface that encloses V_e. It will prove to be convenient to eliminate the F' term in eq A3 because it is responsible for the singular behavior. If we had a single bead of index k and a scalar field equal to a constant, ζ_k, everywhere, then eq A3 reduces to

$$\int_{S_k} F'(\alpha,r)\,dS_x = \Phi(\underline{y},V_{ek}) - \alpha^2 H_k(\alpha,\underline{y}) \qquad \text{(A7)}$$

$$H_k(\alpha,\underline{y}) = \int_{V_{ek}} F(\alpha,r)\,dV_x \qquad \text{(A8)}$$

where V_{ek} denotes the entire volume exterior to bead k. Equation A3 can then be written

$$\Lambda(\underline{y},V_e)\,\Phi(\underline{y},V_e) = -\int_{V_e} F(\alpha,r)\,h(\alpha,\underline{x})\,dV_x - \sum_{k=1}^{N}\int_{S_k} F(\alpha,r)\,p^e(\underline{x})\,dS_x + \sum_{k=1}^{N}\zeta_k[\Phi(\underline{y},V_{ek}) - \alpha^2 H_k(\alpha,\underline{y})] \qquad \text{(A9)}$$

In order to deal with H_k as well as related problems in the present study, it will prove convenient to outline the derivation of a series expansion for eq A4. Consider a closely related expansion (see, e.g., p 768 of ref48) in a reference frame where Ω_x and Ω_y denote the angular coordinates (θ and ϕ) of the vectors $\mathbf{x}$ and $\mathbf{y}$ (of magnitude x and y) in spherical coordinates,

$$\frac{e^{i\gamma r}}{4\pi r} = i\gamma\sum_{n=0}^{\infty}\sum_{m=-n}^{n} j_n(\gamma r_<)\,h_n^{(1)}(\gamma r_>)\,Y^*_{n,m}(\Omega_x)\,Y_{n,m}(\Omega_y) \qquad \text{(A10)}$$

where $i = (-1)^{1/2}$, j_n and $h_n^{(1)}$ are spherical Bessel functions, $Y_{n,m}$ is a spherical harmonic, * denotes complex conjugation, and $r_<$ ($r_>$) is the lesser (greater) of x and y. When $i\gamma = -\alpha$ (a negative real constant), it can be shown

$$F(\alpha,r) = \alpha\sum_{n=0}^{\infty}\sum_{m=-n}^{n} i_n(\alpha r_<)\,k_n(\alpha r_>)\,Y^*_{n,m}(\Omega_x)\,Y_{n,m}(\Omega_y) \qquad \text{(A11)}$$

where i_n and k_n are modified spherical Bessel functions (see pp 531 and 532 of ref 48). The lowest order terms are given by

$$i_0(z) = \frac{\sinh(z)}{z} \qquad \text{(A12)}$$

$$k_0(z) = \frac{e^{-z}}{z} \qquad \text{(A13)}$$

Higher order functions are readily derived from these using straightforward recurrence formulas.[48]

In order to evaluate H_k given by eq A8, the integration is carried out in a reference frame with the origin chosen to coincide with the center of bead k. Making use of the expansion eq A11 in eq A8, we find

$$H_k(\alpha,\underline{y}) = \alpha \int_{a_k}^{\infty} x^2 \, \mathrm{d}x \, i_0(\alpha r_<) \, k_0(\alpha r_>) \tag{A14}$$

Making use of eqs A12 and A13, we find

$$G_k(\alpha,a_k,\underline{y}) = 1 - \alpha^2 H_k(\alpha,\underline{y}) = \frac{k_0(\alpha r_k)}{2}[\mathrm{e}^{\alpha a_k}(\alpha a_k - 1) + \mathrm{e}^{-\alpha a_k}(\alpha a_k + 1)] \tag{A15}$$

where $r_k = |\mathbf{y} - \mathbf{x}_k|$ and $\mathbf{x}_k$ denotes the position of the center of bead k. For a point, $\mathbf{y}$, in the fluid domain or on the surface of any bead, eq A9 becomes

$$\Lambda(\underline{y}) = -\int_{V_e} F(\alpha,r)\, h(\alpha,\underline{x})\, \mathrm{d}V_x - \sum_{k=1}^{N} \int_{S_k} F(\alpha,r)\, p^{\mathrm{e}}(\underline{x})\, \mathrm{d}S_x + \sum_{k=1}^{N} \zeta_k G_k(\alpha,a_k,\underline{y}) \tag{A16}$$

For a weakly charged bead array, the exponential in eq A1 can be expanded, and retaining the leading nonvanishing term yields the linear Poisson−Boltzmann equation,

$$\nabla^2 \Lambda(\underline{x}) \approx \kappa^2 \Lambda(\underline{x}) \tag{A17}$$

$$\kappa^2 = \frac{\beta C q^2}{\epsilon_w} \sum_j c_{j0} z'^2_j \tag{A18}$$

where κ is the Debye−Huckel screening parameter. Using eq A17 in eq A5 and choosing $\alpha = \kappa$, we find that the volume integral in eq 16 vanishes. Then making use of eq A2, we find eq A16 becomes

$$\Lambda(\underline{y}) = \frac{C}{\epsilon_w} \sum_{k=1}^{N} \int_{S_k} F(\kappa,r)\, \sigma(\underline{x})\, \mathrm{d}S_x + \sum_{k=1}^{N} \zeta_k G_k(\kappa,a_k,\underline{y}) \tag{A19}$$

Approximate σ in the surface integrals with their average values, $qz_k/(4\pi a_k^2)$. Again making use of eq A11 in the surface integrals, we see

$$\Lambda(\underline{y}) = \frac{\kappa q C}{4\pi\epsilon_w} \sum_{k=1}^{N} z_k i_0(\kappa a_k)\, k_0(\kappa r_k) + \sum_{k=1}^{N} \zeta_k G_k(\kappa,a_k,\underline{y}) \tag{A20}$$

Next, consider the special case of a field point, $\mathbf{y}$, on the surface of a particular bead, j. Averaging $k_0(\kappa r_k)$ over the surface of bead j using the identity $F(\kappa,r) = \kappa k_0(\kappa r)/(4\pi)$ and eqs A11 and A13 provides

$$\langle k_0(\kappa r_k)\rangle_{S_j} = \begin{pmatrix} k_0(\kappa a_k) & j = k \\ i_0(\kappa a_j)\, k_0(\kappa r_{jk}) & j \neq k \end{pmatrix} \tag{A21}$$

where $r_{jk} = |\mathbf{x}_j - \mathbf{x}_k|$. Averaging the left-hand side of eq A20 gives ζ_j. It then follows that

$$\sum_{k=1}^{N} A_{jk} \zeta_k = \frac{\kappa q C}{4\pi\epsilon_w} \sum_{k=1}^{N} B_{jk} z_k \tag{A22}$$

where

$$A_{jk} = \begin{pmatrix} 1 - k_0(\kappa a_k)\, s(\kappa a_k)/2 & j = k \\ -i_0(\kappa a_j)\, k_0(\kappa r_{jk})\, s(\kappa a_k)/2 & j \neq k \end{pmatrix} \tag{A23}$$

$$B_{jk} = \begin{pmatrix} i_0(\kappa a_k)\, k_0(\kappa a_k) & j = k \\ i_0(\kappa a_j)\, i_0(\kappa a_k)\, k_0(\kappa r_{jk}) & j \neq k \end{pmatrix} \tag{A24}$$

$$s(\kappa a_k) = \mathrm{e}^{\kappa a_k}(\kappa a_k - 1) + \mathrm{e}^{-\kappa a_k}(\kappa a_k + 1) \tag{A25}$$

It is straightforward to construct $N \times N$ matrices, $\mathbf{A}$ and $\mathbf{B}$, with components given by eqs A23 and A24 and also to define $N \times 1$ column vectors, $\boldsymbol{\zeta}$ and $\mathbf{z}$, respectively. Let $\mathbf{A}^{-1}$ denote the inverse matrix of $\mathbf{A}$. From eq A22, it can be shown

$$\underline{\zeta} = \frac{\kappa q C}{4\pi\epsilon_w} \underline{\underline{\mathbf{A}}}^{-1} \cdot \underline{\underline{\mathbf{B}}} \cdot \underline{\mathbf{z}} \tag{A26}$$

In the fluid domain, the potential can be written

$$\Lambda(\underline{y}) = \frac{qC}{\epsilon_w} \sum_{j=1}^{N} h_j F(\kappa,r_j) \tag{A27}$$

where $r_j = |\mathbf{y} - \mathbf{x}_j|$ and

$$h_j = z_j i_0(\kappa a_j) + \frac{s(\kappa a_j)}{2} \sum_{n,m=1}^{N} A^{-1}_{jn} B_{nm} z_m \tag{A28}$$

The external force per unit volume, $\mathbf{s}_{\mathrm{ext}}(\mathbf{y})$, at point $\mathbf{y}$ in the fluid domain arises from the interaction of local ion densities with a constant external electric field, E. As discussed previously,[7] we can approximate this external force for a weakly charged bead array

$$\underline{s}_{\mathrm{ext}}(\underline{y}) \approx -q\kappa^2 \underline{E} \sum_{j=1}^{N} h_j F(\kappa,r_j) \tag{A29}$$

The principal objective of this appendix has been to account for the effect of finite bead size in the calculation of Λ. In the limit $\kappa a_j \ll 1$ and when only terms to first order in κa_j are retained,

$$A_{jk} \approx \delta_{jk} \tag{A30}$$

$$B_{jk} \approx \begin{pmatrix} (1 - \kappa a_k)/(\kappa a_k) & j = k \\ k_0(\kappa r_{jk}) & j \neq k \end{pmatrix} \tag{A31}$$

Under these conditions, eq A26 simplifies to

$$\zeta_j = \frac{qC}{4\pi\epsilon_w}\left[\frac{z_j}{a_j}(1 - \kappa a_j) + \sum_{k\neq j=1}^{N} \frac{z_k}{r_{jk}} \mathrm{e}^{-\kappa r_{jk}}\right] \tag{A32}$$

Appendix B: Mobility of a Weakly Charged Bead Array

Beginning with the Lorentz reciprocal theorem[49] and the singular solution of a point charge in a salt solution,[50] we show it to be straightforward that the general expression for the fluid velocity in the vicinity of our bead array can be written[7]

$$\underline{v}(\underline{y})\,\Phi(\underline{y},V_e) = \int_{V_e}[\underline{\underline{\mathbf{U}}}(\kappa,\underline{r})\cdot\underline{s}_{ext}(\underline{x}) + \kappa^2 F(\kappa,r)\,\underline{v}(\underline{x})]\,dV_x + \sum_{j=1}^{N}\int_{S_j}\underline{\underline{\mathbf{U}}}(\kappa,\underline{r})\cdot\underline{f}(\underline{x})\,dS_x + \sum_{j=1}^{N}\underline{v}_{j0}[\Phi(\underline{y},V_{ej}) - \kappa^2\int_{V_{ej}}F(\kappa,r)\,dV_x] \quad (B1)$$

where $\mathbf{v}(\mathbf{y})$ is the fluid velocity at field point $\mathbf{y}$, Φ was defined following eqs A3−A6, κ is the Debye−Huckel screening parameter (see eq A18), $\mathbf{r} = \mathbf{x} - \mathbf{y}$, V_e denotes the volume exterior to the entire bead array, V_{ej} denotes the entire volume exterior to bead j, $\mathbf{s}_{ext}(\mathbf{x})$ is the external force/unit volume on the fluid at $\mathbf{x}$, $F(\kappa,r)$ is given by eq A4, $\mathbf{f}(\mathbf{x})$ is the hydrodynamic force/unit area exerted by the bead array on the fluid at $\mathbf{x}$, $\mathbf{v}_{j0}$ is the velocity of bead j (assumed uniform over the bead surface), $\mathbf{U}$ is the singular tensor given by[50]

$$\underline{\underline{\mathbf{U}}}(\kappa,\underline{r}) = \frac{1}{4\pi\eta}\left\{\left[w_1(\kappa,r) + \frac{1}{\kappa}w_2(\kappa,r) - \frac{1}{\kappa^2}(v_3(r) - w_3(\kappa,r))\right]\underline{\underline{\mathbf{I}}} + \left[-w_1(\kappa,r) - \frac{3}{\kappa}w_2(\kappa,r) + \frac{3}{\kappa^2}(v_3(r) - w_3(\kappa,r))\right]\underline{\underline{R}}\right\} \quad (B2)$$

$$v_n(r) = \frac{1}{r^n} \quad (B3)$$

$$w_n(\kappa,r) = \frac{e^{-\kappa r}}{r^n} \quad (B4)$$

$$\underline{\underline{R}} = \frac{\underline{\underline{rr}}}{r^2} \quad (B5)$$

η is the solvent viscosity, and $\mathbf{I}$ is the 3×3 identity tensor.

As in previous work, $\mathbf{U}$ is approximated with its orientational average,[7]

$$\langle\underline{\underline{\mathbf{U}}}(\kappa,\underline{r})\rangle_{oa} = \frac{2}{3\eta}F(\kappa,r)\underline{\underline{\mathbf{I}}} \quad (B6)$$

$\mathbf{f}(\mathbf{x})$ in the surface integral in eq B1 is replaced with its average value, $\mathbf{F}_j$, and use is made of eq A15. With these substitutions, eq B1 can be written

$$\underline{v}(\underline{y})\,\Phi(\underline{y},V_e) = \int_{V_e}\left[\frac{2}{3\eta}\underline{s}_{ext}(\underline{x}) + \kappa^2\underline{v}(\underline{x})\right]F(\kappa,r)\,dV_x + \frac{2}{3\eta}\sum_{j=1}^{N}\underline{F}_j\int_{S_j}F(\kappa,r)\,dS_x + \sum_{j=1}^{N}\underline{v}_{j0}[\Omega_j(\underline{y}) + G_j(\kappa,a_j,\underline{y})] \quad (B7)$$

where $\Omega_j(\mathbf{y})$ equals $-1/2$ if $\mathbf{y}$ lies on S_j and 0 otherwise. From eqs A4 and A21,

$$\int_{S_j}F(\kappa,r)\,dS_x = \kappa a_j^2 i_0(\kappa a_j)\,k_0(\kappa r_j) \quad (B8)$$

where $r_j = |\mathbf{y} - \mathbf{x}_j|$ and $\mathbf{x}_j$ denotes the center of bead j. As discussed in Appendix A, the i's and j's represent modified spherical Bessel functions.[48] For $\mathbf{s}_{ext}(\mathbf{x})$, we use eq A29. For the fluid velocity field appearing in the volume integral of eq B7, we approximate it with a linear combination of orientationally pre-averaged "singular" solutions,

$$\underline{v}(\underline{x}) = q\sum_{j=1}^{N}c_j\langle\underline{\underline{\mathbf{U}}}(\kappa,\underline{r})\rangle_{oa}\cdot\underline{E} = \frac{2q}{3\eta}\underline{E}\sum_{j=1}^{N}c_jF(\kappa,r'_j) \quad (B9)$$

where $r'_j = |\mathbf{x} - \mathbf{x}_j|$, E is a constant external electric field, and the c_j's are constants that will be determined from hydrodynamic boundary conditions. Equation B9 is a generalization of our previous analysis[7] where it was assumed that c_j is proportional to the bead charge, qz_j. Using eqs A29, B8, and B9 in eq B7, we find

$$\underline{v}(\underline{y})\,\Phi(\underline{y},V_e) = \frac{2q\kappa^2\underline{E}}{3\eta}\sum_{j=1}^{N}(c_j - h_j)\int_{V_e}F(\kappa,r'_j)\,F(\kappa,r)\,dV_x + \frac{2\kappa a_j^2}{3\eta}\sum_{j=1}^{N}\underline{F}_j i_0(\kappa a_j)\,k_0(\kappa r_j) + \sum_{j=1}^{N}\underline{v}_{j0}[\Omega_j(\underline{y}) + G_j(\kappa,a_j,\underline{y})] \quad (B10)$$

Now choose $\mathbf{y}$ to be some point on the surface of bead k, and average eq B10 over the surface of bead k. Using eqs A4, A13, and A21, we find it straightforward to show

$$\underline{v}_{k0}\chi_k = \sum_{j=1}^{N}\left[\frac{2\kappa a_j^2}{3\eta}W_{kj}^{(1)}\underline{F}_j + \frac{q\kappa}{12\pi\eta}\underline{E}(c_j - h_j)W_{kj}^{(2)}\right] \quad (B11)$$

where

$$\chi_k = 1 - \frac{1}{2}s(\kappa a_k)\,k_0(\kappa a_k) - \frac{1}{2}\sum_{j\neq k}s(\kappa a_j)\,i_0(\kappa a_k)\,k_0(\kappa r_{jk}) \quad (B12)$$

$$W_{kj}^{(1)} = \begin{cases} i_0(\kappa a_k)\,k_0(\kappa a_k) & j = k \\ i_0(\kappa a_k)\,i_0(\kappa a_j)\,k_0(\kappa r_{jk}) & j \neq k \end{cases} \quad (B13)$$

$$W_{kj}^{(2)} = i_0(\kappa a_k)\,I_{jk} \quad (B14)$$

$$I_{jk} = 8\pi\kappa\int_V F(\kappa,r'_j)\,F(\kappa,r'_k)\,dV_x \quad (B15)$$

and $r_{jk} = |\mathbf{x}_j - \mathbf{x}_k|$. For $j = k$,

$$I_{kk} = e^{-2\kappa a_k} - 2\sum_{p\neq k}\sum_{s=0}^{\infty}(2s+1)k_s^2(\kappa r_{kp})\,h_s(\kappa a_p) \quad (B16)$$

and for $j \neq k$,

$$I_{jk} = e^{-\kappa r_{jk}} - k_0(\kappa r_{jk})\left[\kappa(a_j + a_k) - 1 + \frac{1}{2}(e^{-2\kappa a_j} + e^{-2\kappa a_k})\right] - 2\sum_{p\neq j\text{ or }k}\sum_{s=0}^{\infty}(2s+1)k_s(\kappa r_{jp})\,k_s(\kappa r_{kp})\,P'_s(\cos(\gamma_{jp,kp}))h_s(\kappa a_p) \quad (B17)$$

where P_s' is a Legendre polynomial of order s, $\gamma_{jp,kp}$ is the angle between the position vectors $\mathbf{r}_{jp}$ and $\mathbf{r}_{kp}$, and

$$h_s(z) = \int_0^z t^2\,dt\,i_s^2(t) \quad (B18)$$

The lowest order terms of h_s are given by

$$h_0(z) = \frac{-2z + \sinh(2z)}{4} \rightarrow \frac{z^3}{3} + \frac{z^5}{15} + \frac{2z^7}{315} + \frac{z^9}{2835} \quad (B19)$$

$$h_1(z) = \frac{2 + 2z^2 - 2\cosh(2z) + z\sinh(2z)}{4z} \rightarrow \frac{z^5}{45} + \frac{z^7}{315} + \frac{z^9}{4725} \quad (B20)$$

$$h_2(z) = [(6 - 6z^2 - 2z^4) - (6 + 6z^2)\cosh(2z) + (12z + z^3)\sinh(2z)]/4z^3 \rightarrow \frac{z^7}{1575} + \frac{z^9}{14\,175} \quad \text{(B21)}$$

$$h_3(z) = [(90 - 30z^2 + 12z^4 - 2z^6) - (90 + 150z^2 + 12z^4)\cosh(2z) + (180z + 60z^3 + z^5)\sinh(2z)]/4z^5 \rightarrow \frac{z^9}{99\,225} \quad \text{(B22)}$$

The polynomials (pointed to by the arrows) in eqs B19−B22 represent series expansions, out to order z^{10}, which are valid for small z. These polynomial expansions illustrate how rapidly the h_s terms fall off with increasing $z = \kappa a$ where a is a typical bead radius. If $\kappa a \ll 1$ and only terms to order $(\kappa a)^2$ are included, all of the terms that involve h_s in eqs B16 and B17 vanish, and

$$I_{kj} \approx \begin{pmatrix} e^{-2\kappa a_k} & j = k \\ e^{-\kappa r_{jk}}\left(1 + \frac{\kappa(a_j^2 + a_k^2)}{r_{jk}}\right) & j \neq k \end{pmatrix} \quad \text{(B23)}$$

For the cases of interest in this work, κa is less than approximately 2, and only the lowest order terms, h_s, contribute to eqs B16 and B17. Terms of order $s \leq 3$ are included in this work.

In electrophoresis, all of the beads migrate with the same velocity. Since the hydrodynamic interation tensor, **U**, has been orientationally averaged, we can write

$$\underline{v}_{j0} = \mu \underline{E} \quad \text{(B24)}$$

where μ is the electrophoretic mobility of the bead array. In order to evaluate the c_j's appearing in eq B9, it is averaged over the surface of bead k, and use is made of eq A21

$$\frac{6\pi\eta\mu}{q\kappa} = \sum_{j=1}^{N} X_{kj} c_j \quad \text{(B25)}$$

where

$$X_{kj} = \begin{pmatrix} k_0(\kappa a_k) & j = k \\ i_0(\kappa a_k)\, k_0(\kappa r_{jk}) & j \neq k \end{pmatrix} \quad \text{(B26)}$$

Once a structure has been defined, the $N \times N$ matrix, **X**, formed by the components given by eq B26 can be readily inverted to yield the inverse matrix, $\mathbf{X}^{-1}$. Defining

$$d_k = \sum_{j=1}^{N} X_{kj}^{-1} \quad \text{(B27)}$$

we have

$$c_k = \frac{6\pi\eta\mu}{q\kappa} d_k \quad \text{(B28)}$$

It is still necessary, however, to determine μ. Returning to eq B11, we find it convenient to define the dimensionless hydrodynamic forces, g_k, by the identity

$$S_k \underline{F}_k = q g_k \underline{E} \quad \text{(B29)}$$

where $S_k = 4\pi a_k^2$ is the surface area of bead k. Using eqs B24, B28, and B29 in eq B11 and rearranging, we find

$$\mu\left(\chi_k - \frac{1}{2}\sum_{j=1}^{N} W_{kj}^{(2)} d_j\right) = \frac{q\kappa}{6\pi\eta}\sum_{j=1}^{N}\left[W_{kj}^{(1)} g_j - \frac{1}{2} W_{kj}^{(2)} h_j\right] \quad \text{(B30)}$$

Next, define

$$S_T = \sum_{j=1}^{N} S_j \quad \text{(B31)}$$

$$m_k = S_k / S_T \quad \text{(B32)}$$

$$P_1^{(k)} = \sum_{j=1}^{N} m_j W_{kj}^{(1)} \quad \text{(B33)}$$

$$P_2^{(k)} = \sum_{j=1}^{N} h_j W_{kj}^{(2)} \quad \text{(B34)}$$

$$P_3^{(k)} = \sum_{j=1}^{N} d_j W_{kj}^{(2)} \quad \text{(B35)}$$

$$\chi = \sum_{k=1}^{N} m_k \chi_k \quad \text{(B36)}$$

$$P_s = \sum_{k=1}^{N} m_k P_s^{(k)} \quad \text{(B37)}$$

With these definitions, eq B30 becomes

$$\mu\left(\chi_k - \frac{1}{2} P_3^{(k)}\right) = \frac{q\kappa}{6\pi\eta}\left(\sum_{j=1}^{N} W_{kj}^{(1)} g_j - \frac{1}{2} P_2^{(k)}\right) \quad \text{(B38)}$$

Multiply eq B38 by m_k, and sum over k

$$\mu = \frac{q\kappa}{6\pi\eta}\left(\sum_{j=1}^{N} P_1^{(j)} g_j - \frac{1}{2} P_2\right) \Big/ \left(\chi - \frac{1}{2} P_3\right) \quad \text{(B39)}$$

What are unknown in eq B39 are the g_j's. Use eq B39 in eq B38 to eliminate μ. Straightforward rearrangement yields

$$\underline{\underline{\mathbf{D}'}} \cdot \mathbf{g} = \underline{\xi'} \quad \text{(B40)}$$

where **g** is an $N \times 1$ column vector consisting of the elements, g_j, ξ' is an $N \times 1$ column vector with elements

$$\xi_k' = \frac{1}{2} P_2\left(\chi_k - \frac{1}{2} P_3^{(k)}\right) - \frac{1}{2} P_2^{(k)}\left(\chi - \frac{1}{2} P_3\right) \quad \text{(B41)}$$

and $\mathbf{D}'$ is an $N \times N$ matrix with elements

$$D_{kj}' = \left(\chi_k - \frac{1}{2} P_3^{(k)}\right) P_1^{(j)} - \left(\chi - \frac{1}{2} P_3\right) W_{kj}^{(1)} \quad \text{(B42)}$$

It is not possible to solve eq B40 because the inverse of $\mathbf{D}'$ does not exist. As discussed previously,[7] we have an additional relation which arises when one considers the overall force balance on the bead array

$$\sum_{j=1}^{N} g_j = \sum_{j=1}^{N} z_j = z_T \quad \text{(B43)}$$

Multiply eq B43 by an arbitrary constant, λ_k, and subtract this from eq B40 for component k

$$\sum_{j=1}^{N}(D_{kj}' - \lambda_k)g_j = \xi_k' - \lambda_k z_T \tag{B44}$$

Choose $\lambda_k = D_{kk}'$ and define

$$D_{kj} = D_{kj}' - D_{kk}' \tag{B45}$$

$$\xi_k = \xi_k' - D_{kk}' z_T \tag{B46}$$

With these definitions, we now have

$$\underline{\underline{\mathbf{D}}}\cdot\mathbf{g} = \underline{\xi} \tag{B47}$$

Unlike $\mathbf{D}'$, $\mathbf{D}$ is invertible, and the components of $\mathbf{g}$ are given by

$$\mathbf{g} = \underline{\underline{\mathbf{D}}}^{-1}\cdot\underline{\xi} \tag{B48}$$

In summary, once a structure is defined, it is possible to compute $\mathbf{D}^{-1}$, $\boldsymbol{\xi}$, and hence $\mathbf{g}$. Finally, eq B39 is used to compute the mobility.

References and Notes

(1) Messana, I.; Rossetti, D. V.; Cassiano, L.; Misiti, F.; Giardina, B.; Castagnola, M. *J. Chromatogr., B* **1997**, *699*, 149.
(2) Offord, R. E. *Nature (London)* **1966**, *211*, 591.
(3) Jalali-Heravi, M.; Shen, Y.; Hassanisadi, M.; Khaledi, M. G. *Electrophoresis* **2005**, *26*, 874.
(4) Janini, G. M.; Metral, C. J.; Issaq, H. J.; Muschik, G. M. *J. Chromatogr.* **1999**, *848*, 417.
(5) Janini, G. M.; Metral, C. J.; Issaq, H. J. *J. Chromatogr., A* **2001**, *924*, 291.
(6) Jalali-Heravi, M.; Shen, Y.; Hassanisadi, M.; Khaledi, M. G. *J. Chromatogr., A* **2005**, *1096*, 58.
(7) Allison, S.; Xin, Y.; Mitchell, H. *Recent Res. Dev. Macromol. Res.* **2005**, *8*, 25.
(8) Xin, Y.; Mitchell, H.; Cameron, H.; Allison, S. *J. Phys. Chem. B* **2006**, *110*, 1038.
(9) Hunter, R. J. *Introduction to Modern Colloid Science;* Oxford University Press: Oxford, U.K., 2002; Chapter 7.
(10) Allison, S. A.; Carbeck, J. D.; Chen, C.; Burkes, F. *J. Phys. Chem. B* **2004**, *108*, 4516.
(11) Overbeek, J. T. G. *Kolloid−Beih.* **1943**, *54*, 287.
(12) Booth, F. *Proc. R. Soc. London, Ser. A* **1950**, *203*, 514.
(13) Wiersema, P. H.; Loeb, A. L.; Overbeek, J. T. G. *J. Colloid Interface Sci.* **1966**, *22*, 78.
(14) O'Brien, R. W.; White, L. R. *J. Chem. Soc., Faraday Trans. 2* **1978**, *74*, 1607.
(15) Carbeck, J. D.; Colton, I. J.; Anderson, J. R.; Deutch, J. M.; Whitesides, G. M. *J. Am. Chem. Soc.* **1999**, *121*, 10 671.
(16) Allison, S.; Chen, C.; Stigter, D. *Biophys. J.* **2001**, *81*, 2558.
(17) Aragon, S.; Hahn, D. K. *Biophys. J.* **2006**, *91*, 1591.
(18) Flory, P. J. *Statistical Mechanics of Chain Molecules*; Wiley: New York, 1969; Chapter 7.
(19) Antosiewicz, J.; Porschke, D. *J. Phys. Chem.* **1989**, *93*, 5301.
(20) Kim, J. Y.; Ahn, S. H.; Kang, S. T.; Yoon, B. J. *J. Colloid Interface Sci.* **2006**, *299*, 486.
(21) Linderstrom-Lang, K. C. *C. R. Trav. Lab. Carlsberg* **1924**, *15*, 1.
(22) Lee, L. K.; Fitch, C. A.; Garcia-Moreno, B. E. *Protein Sci.* **2002**, *11*, 1004.
(23) Carbeck, J. D.; Negin, R. S. *J. Am. Chem. Soc.* **2001**, *123*, 1252.
(24) Garcia de la Torre, J.; Bloomfield, V. A. *Q. Rev. Biophys.* **1981**, *14*, 81.
(25) Garcia de la Torre, J.; Navarro, S.; Lopez-Martinez, M. C.; Diaz, F. G.; Lopez-Casales, J. J. *Biophys. J.* **1994**, *67*, 530.
(26) Allison, S. *J. Colloid Interface Sci.* **2005**, *282*, 231.
(27) Allison, S.; Potter, M.; McCammon, J. A. *Biophys. J.* **1997**, *73*, 133.
(28) Rickard, E. C.; Strohl, M. M.; Nielsen, R. G. *Anal. Biochem.* **1991**, *197*, 197.
(29) Compton, B. J. *J. Chromatogr.* **1991**, *559*, 357.
(30) Issaq, H. J.; Janini, G. M.; Atamna, I. Z.; Muschik, G. M.; Lukszo, J. *J. Liq. Chromatogr.* **1992**, *15*, 1129.
(31) Castagnola, M.; Cassiano, L.; Messana, I.; Nocca, G.; Rabino, R.; Rossetti, D. V.; Giardina, B. *J. Chromatogr., B* **1994**, *656*, 87.
(32) Cifuentes, A.; Poppe, H. *J. Chromatogr., A* **1994**, *680*, 321.
(33) Basak, S. K.; Ladisch, M. R. *Anal. Biochem.* **1995**, *226*, 51.
(34) Adamson, N. J.; Reynolds, E. C. *J. Chromatogr., B* **1997**, *699*, 133.
(35) Messana, I.; Rossetti, D. V.; Cassiano, L.; Misiti, F.; Giardina, B.; Castagnola, M. *J. Chromatogr., B* **1997**, *699*, 149.
(36) Kim, J.; Zand, R.; Lubman, D. M. *Electrophoresis* **2002**, *23*, 782.
(37) Allison, S. A. *Biophys. Chem.* **2001**, *93*, 197.
(38) Allison, S. *Macromolecules* **1996**, *29*, 7391.
(39) Stigter, D. *J. Phys. Chem.* **1978**, *82*, 1417, 1424.
(40) Hagerman, P. J.; Zimm, B. H. *Biopolymers* **1981**, *20*, 1481.
(41) Kirkwood, J. G. In *Macromolecules;* Auer, P. L., Ed.; Gordon and Breach: New York, 1967.
(42) Garcia de la Torre, J.; Bloomfield, V. A. *Biopolymers* **1977**, *16*, 1747.
(43) Teller, D. C.; Swanson, E.; de Haen, C. *Methods Enzymol.* **1979**, *61*, 103.
(44) Garcia de la Torre, J.; Jimenez, A.; Freire, J. J. *Macromolecules* **1982**, *15*, 148.
(45) Aragon, S.; Kahn, D. K. *J. Chem. Theory Comput.* **2006**, *2*, 12.
(46) Juffer, A. H.; Botta, E. F. F.; Van Keulen, B. A. M.; Van Der Ploeg, A.; Berendsen, H. J. C. *J. Comput. Phys.* **1991**, *97*, 144.
(47) Zhou, H.-X. *J. Chem. Phys.* **1994**, *100*, 3152.
(48) Arfken, G. *Mathematical Methods for Physicists;* Academic Press: New York, 1970.
(49) Kim, S.; Karrila, S. J. *Microhydrodynamics: Principles and Selected Applications;* Butterworth-Heinemann: Boston, MA, 1991; Section 2.3.
(50) Allison, S. A.; Stigter, D. *Biophys. J.* **2000**, *78*, 121.